MS-I

GPO PRICE $ _____

OTS PRICE(S) $ _____

Hard copy (HC) 2.00

Microfiche (MF) .50

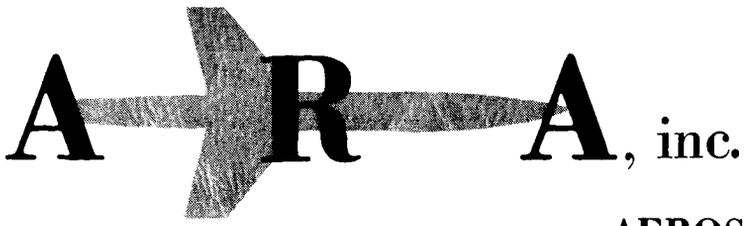

AEROSPACE RESEARCH ASSOCIATES

2017 WEST GARVEY AVENUE • WEST COVINA, CALIFORNIA 91790 • TEL. 962-1045

Final Report

on

"High Energy Shock Absorber and Structural

Overload Devices"

Contract Number: NAS 8-11687

ARA Report No. 60

Approved by:

Bernard Mazelsky, President, ARA, Inc.

4 June 1965

TABLE OF CONTENTS

Foreword

The research and development work described herein was performed by ARA, Inc., West Covina, California, for the George C. Marshall Space Flight Center, National Aeronautics and Space Administration, under Contract NAS 8-11687, "High Energy Shock Absorber and Structural Overload Devices."

The work began in July, 1964, and was concluded in May, 1965. Mr. Bernard Mazelsky was the Program Manager and Dr. D. L. Platus was the Principal Investigator. Although the work was a group effort, the chief contributors were Dr. D. L. Platus, who developed the theory and design procedures, and Mr. P. J. Cunningham, who directed the laboratory testing, design, and fabrication effort. They were assisted by Mr. H. H. Freeman, Mr. C. G. Daniels, Mr. F. A. Marovich and Mr. Bernard Mazelsky.

LIST OF FIGURES

LIST OF TABLES

I SUMMARY

27374

Results of an 11-month research and development program are described which cover an analytical and experimental study and the design and fabrication of five advanced energy absorbing devices, utilizing the principle of cyclic deformation of materials. The study represents a continuation of research on cyclic-strain energy-absorbing devices previously conducted at ARA, Inc.

Energy absorption, fatigue, and plastic stability of rotating torus segments were studied analytically and experimentally, using rotating beam tests. Design procedures for torus devices utilizing friction drive are presented. These results were applied to the design and fabrication of energy absorber units providing up to 53,300 lb force over a 36-inch stroke, and capable of multiple operation in tension and compression.

Author

II INTRODUCTION

The principles of cyclic-strain energy-absorbing devices have been previously described (Reference 1). Devices of this type operate by converting unidirectional mechanical energy into cyclic deformation of a working material, such as a ductile metal, and offer significant advantages over other energy absorbing systems currently under study. They can be designed to provide constant or varying load-stroke curves, high reliability, multiple-use capability in tension and compression, and high weight and volume efficiencies.

The objectives of this program were: (1) to continue the research on cyclic-strain energy-absorbing devices previously conducted at ARA, Inc. and

provide basic design data; (2) to apply the results to the design and fabrication of energy absorber units to meet specific design requirements. Five units were required, the largest to provide a 53,300 lb force over a 36-inch stroke.

An attractive design approach utilizes the rolling of toroidal elements to convert unidirectional mechanical energy into cyclic strain energy. In one variation of the approach the torus elements are driven in friction contact between two concentric tubes. A limited investigation of this approach is described in Reference 1. It is shown that lateral deformation of the elements required for adequate friction drive gives rise to a complicated stress state and increased energy absorption.

Another variation on the torus approach utilizes torus segments, mounted and driven in a manner similar to a specimen in a rotating-beam test. A considerable portion of the analytical and experimental study phase of the program was directed toward an investigation of the energy absorption, fatigue, and plastic stability of rotating torus segments. However, because of the success obtained with the complete torus and friction drive approach under another development program, and the relative simplicity of this approach, it was decided to utilize this approach in the design and fabrication phase of the program.

In the following sections, analyses and design data for both the torus segment and friction drive approach are presented, and application of the friction drive results to the design and fabrication of several energy absorber units is described.

III ANALYSIS

A. Torus Segment Approach

The original design concept considered for the energy absorbers utilized working elements in the form of torus segments supported on bearings in such a manner that the curvature and, hence, the force level could be continuously adjusted. This mode of operation raised certain questions regarding the applied forces, energy absorption parameters, fatigue life, and stability of the working elements. A brief analysis of these problems is presented below.

1. Load Distributions

Consider a solid torus segment of length ℓ and diameter d, supported on bearings and driven at one end, as shown in Figure 1. The driving torque T_m applied at B produces a reacting force F at A, normal to the plane of the segment. This force gives rise to distributions of torque T and bending moment M along the segment, given by

$$\left.\begin{aligned} T(\theta) &= Fy(\theta) = FR(1 - \cos\theta) \\ M(\theta) &= Fx(\theta) = FR\sin\theta \end{aligned}\right\}, \qquad (1)$$

where x and y are moment arms, as indicated in the figure, θ is the angular coordinate, and R is the radius of curvature. The maximum values of T and M are given by

$$\left.\begin{aligned} T_m &= Fb = FR(1 - \cos\theta_m) \\ M_m &= Fa = FR\sin\theta_m \end{aligned}\right\}. \qquad (2)$$

The distributions may be normalized to their maximum values, to give

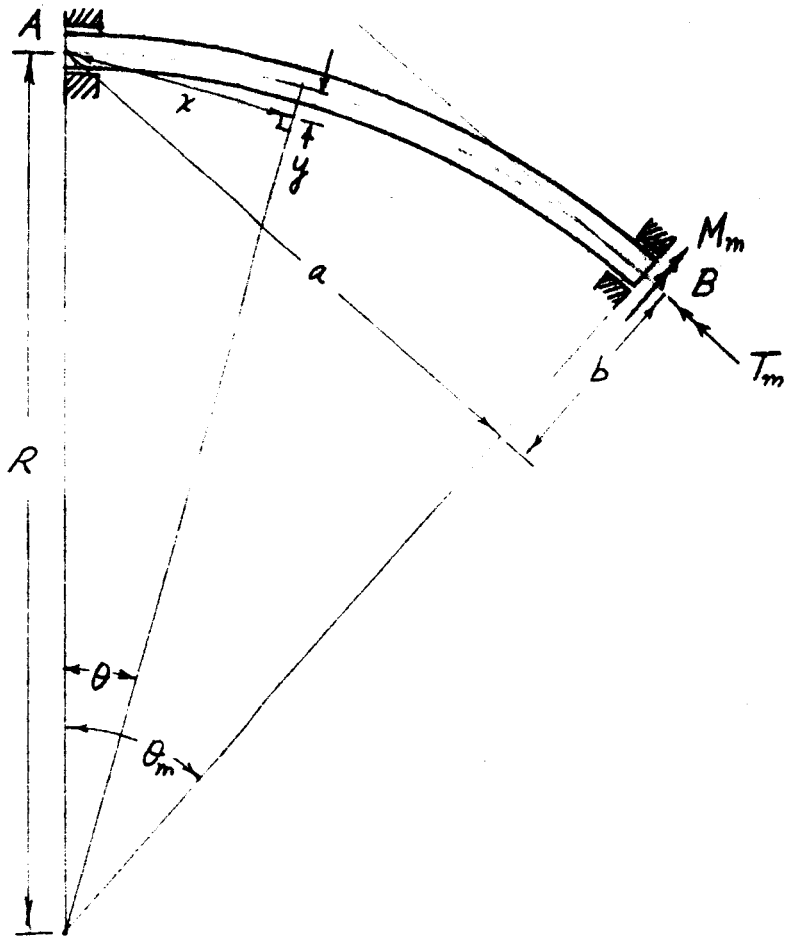

Figure 1. Rotating Torus Segment

$$\frac{T}{T_m} = \frac{1 - \cos\theta}{1 - \cos\theta_m} \quad , \quad \frac{M}{M_m} = \frac{\sin\theta}{\sin\theta_m} \; . \tag{3}$$

For small values of θ , Equations (2) and (3) yield

$$\frac{T}{T_m} \simeq \frac{\theta^2}{\theta_m^2} \quad , \quad \frac{M}{M_m} = \frac{\theta}{\theta_m} \quad , \quad \frac{M}{T_m} = \frac{2\theta}{\theta_m^2} \; . \tag{4}$$

Thus, it is seen that, for small θ_m, both T and M are proportional to T_m, T varies as the square of θ , and M is linear with θ .

The presence of these torque and moment distributions affect the performance of the elements by producing variations in the stress states from those of simple bending. The torques produce steady shear stresses in the direction of rotation which are superimposed on the cyclic bending stresses; the moments produce variations in the cyclic bending stresses due to the rotation of the elements.

It has been shown (References 2 and 3) that the presence of small steady stresses during cyclic straining of a ductile metal can give rise to significant plastic deformation in the direction of the steady stresses. Moyar and Sinclair (Reference 2) subjected tubular specimens of copper to small steady tensions and alternating torsion, and observed appreciable accumulations of axial strain. Moreover, the presence of small axial tension caused a significant reduction in the fatigue life based on the torsional straining alone. Results of Moyar and Sinclair's tests are shown in Table 1 and Figure 2. The figure shows the effect of a steady axial stress σ_o on the reduction in the fatigue constant C in

Table 1. Low-Cycle Fatigue of Copper Under Steady Tension and Alternating Torsion
(Moyar and Sinclair, 1963)

Specimen Number	Axial Stress (psi)	Shear Strain Range	Maximum Shear Stress Range (psi)	Minimum Plastic Shear Strain Range	Axial Fracture Strain	Cycles to Fracture	Notes
3-s	11,000	0.0148	29,000	0.0092	0.306	509	Dimen. Inst. after N = 160
2-s	7,000	0.0144	27,200	0.0092	0.247	968	Dimen. Inst. after N = 630
5-s	4,500	0.0145	22,900	0.0098	0.259	2,141	Dimen. Inst. after N = 1,350
4-s	2,000	0.0147	20,100	0.0103	0.141	2,802	
6-s	11,000	0.0115	27,100	0.0062	0.315	1,685	Dimen. Inst. after N = 440
8-s	7,000	0.0116	23,300	0.0066	0.262	2,871	Dimen. Inst. after N = 1,460
9-s	4,500	0.0108	21,400	0.0068	0.178	2,922	
7-s	2,000	0.0112	19,000	0.0070	0.097	5,206	
24-s	11,000	0.0091	23,900	0.0045	0.234	1,336	Dimen. Inst. after N = 900
23-s	7,000	0.0092	22,200	0.0049	0.251	5,722	Dimen. Inst. after N = 3,400
22-s	4,500	0.0094	20,800	0.0051	0.140	4,078	Failure at grip
15-s	2,000	0.0093	19,000	0.0058	0.074	8,523	
18-s	11,000	0.0069	20,900	0.0032	0.256	5,045	Dimen. Inst. after N = 2,400
17-s	7,000	0.0072	19,400	0.0035	0.193	9,661	
20-s	4,500	0.0073	18,200	0.0036	0.146	13,477	
14-s	2,000	0.0072	15,400	0.0038	0.053	17,787	
19-s	11,000	0.0053	17,000	0.0019	0.174	10,073	
10-s	7,000	0.0056	16,300	0.0021	0.114	15,418	
21-s	4,500	0.0055	14,000	0.0026	0.069	21,277	
13-s	2,000	0.0057	12,300	0.0030	0.033	38,950	

Figure 2. Effect of Axial Tension on Low-Cycle Fatigue of Copper in Torsion
(Data from Moyar and Sinclair, 1963)

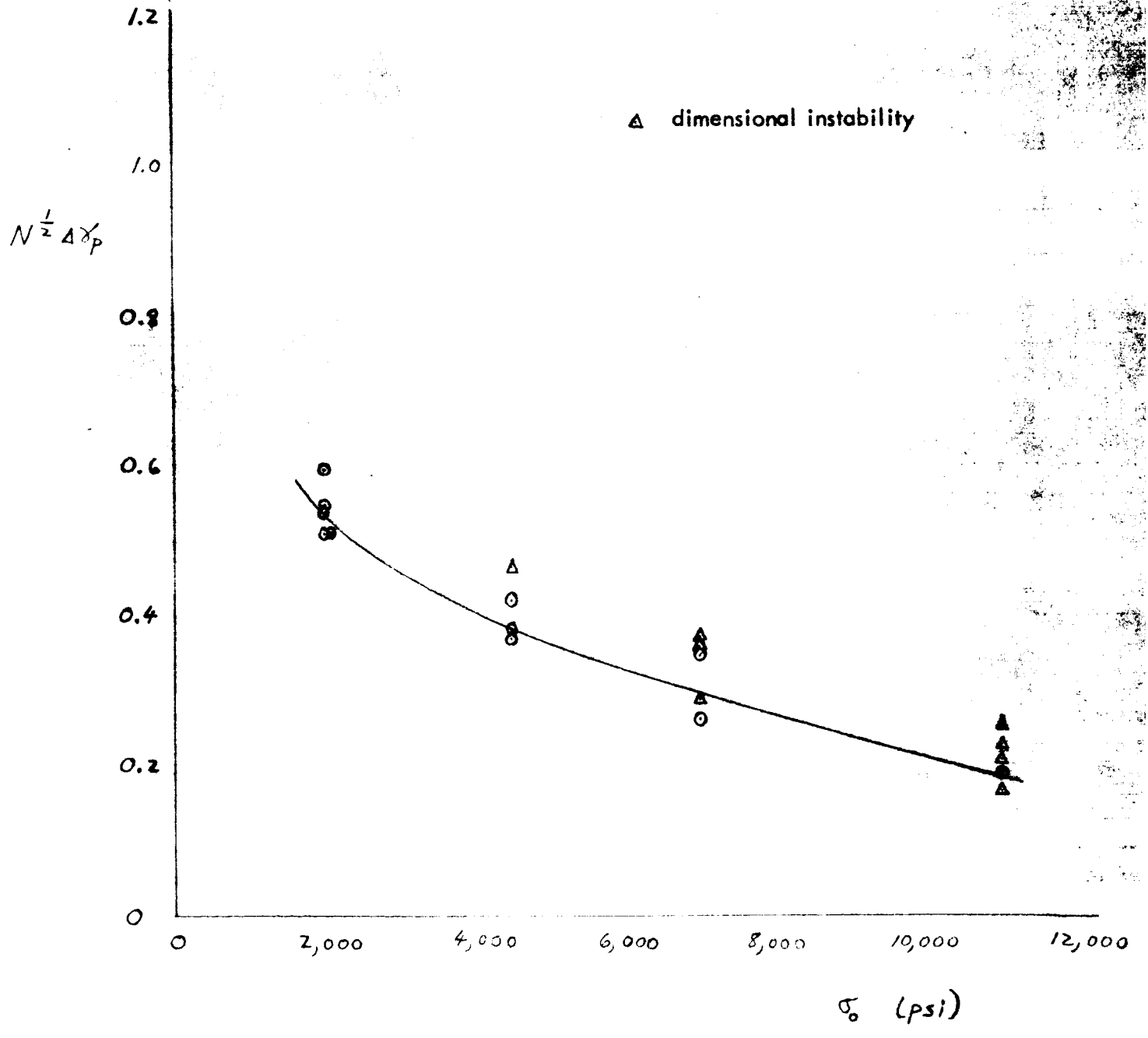

Coffin's empirical relation (Reference 4),

$$N^{1/2} \Delta\gamma_p = C, \tag{5}$$

where N is the fatigue life and $\Delta\gamma_p$ is the plastic strain range in torsion. It has been shown that the constant C is proportional to fracture ductility, as determined in a tensile test. If it is assumed that the ductility is reduced due to the combined stress effects resulting from the steady tension, and that the fatigue life is affected accordingly, then the quantity $N^{1/2} \Delta\gamma_p$ should correlate with the axial stress, independent of strain range. The correlation of Figure 2 seems to be quite good, considering the scatter normally associated with fatigue failures.

2. Energy Absorption and Fatigue Relations

Before investigating the plastic stability of the rotating torus segments, it is convenient to establish the energy absorption and fatigue parameters based on the bending deformation alone. An energy balance yields

$$2\pi T_m = \int_{\text{element}} w_p \, dV, \tag{6}$$

where $\bar{w}_p$ is the area under the hysteresis loop, or energy absorbed per unit volume per cycle, and V is the volume of the element. The integral may be written,

$$\int w_p \, dV = \bar{w}_p V = \eta \, \Delta\sigma \, \Delta\epsilon_p V \quad , \tag{7}$$

where $\bar{w}_p$ is the average hysteresis loop; $\Delta\sigma$ and $\Delta\epsilon_p$ are the maximum values of stress range and plastic strain range, respectively; and η is an efficiency factor which relates $\bar{w}_p$ to the basic material cyclic-strain properties, $\Delta\sigma$ and $\Delta\epsilon_p$. With $V = \pi d^2 \ell / 4$, Equations (6) and (7) give

$$T_m = \frac{\eta}{8} d^2 \ell \Delta\sigma \Delta\epsilon_p \quad . \tag{8}$$

Introducing the total strain range,

$$\Delta\epsilon_T = \frac{d}{R} \quad , \tag{9}$$

and modulus of elasticity, E, Equation (8) may be written

$$T_m = \frac{\eta}{8} d^2 \ell \Delta\sigma \left(\frac{d}{R} - \frac{\Delta\sigma}{E} \right) . \tag{10}$$

The fatigue life can be determined from Coffin's empirical relation, written for tension-compression,

$$N^{1/2} \Delta\epsilon_p = C \quad , \tag{11}$$

where C is a constant for the material.

Equations (8) - (11) provide a convenient set of relations which can be used to study the effects of torque and moment distributions on the energy absorption and fatigue behavior of rotating torus segments. These relations are used in conjunction with basic cyclic stress-strain properties, such as those for type 347 stainless steel, shown in Figure 3. A major objective of the test program described in Section IV was to determine η and N as a function of the various design parameters such as strain range, element length, and element diameter.

3. Plastic Stability

The steady torsional stresses in the rotating torus segment are analogous to the steady axial tensions in Moyar and Sinclair's tests, and can

Figure 3. Cyclic Stress-Strain Data for 347 Stainless Steel (solution treated) (Data from Coffin and Tavernelli, Reference 2)

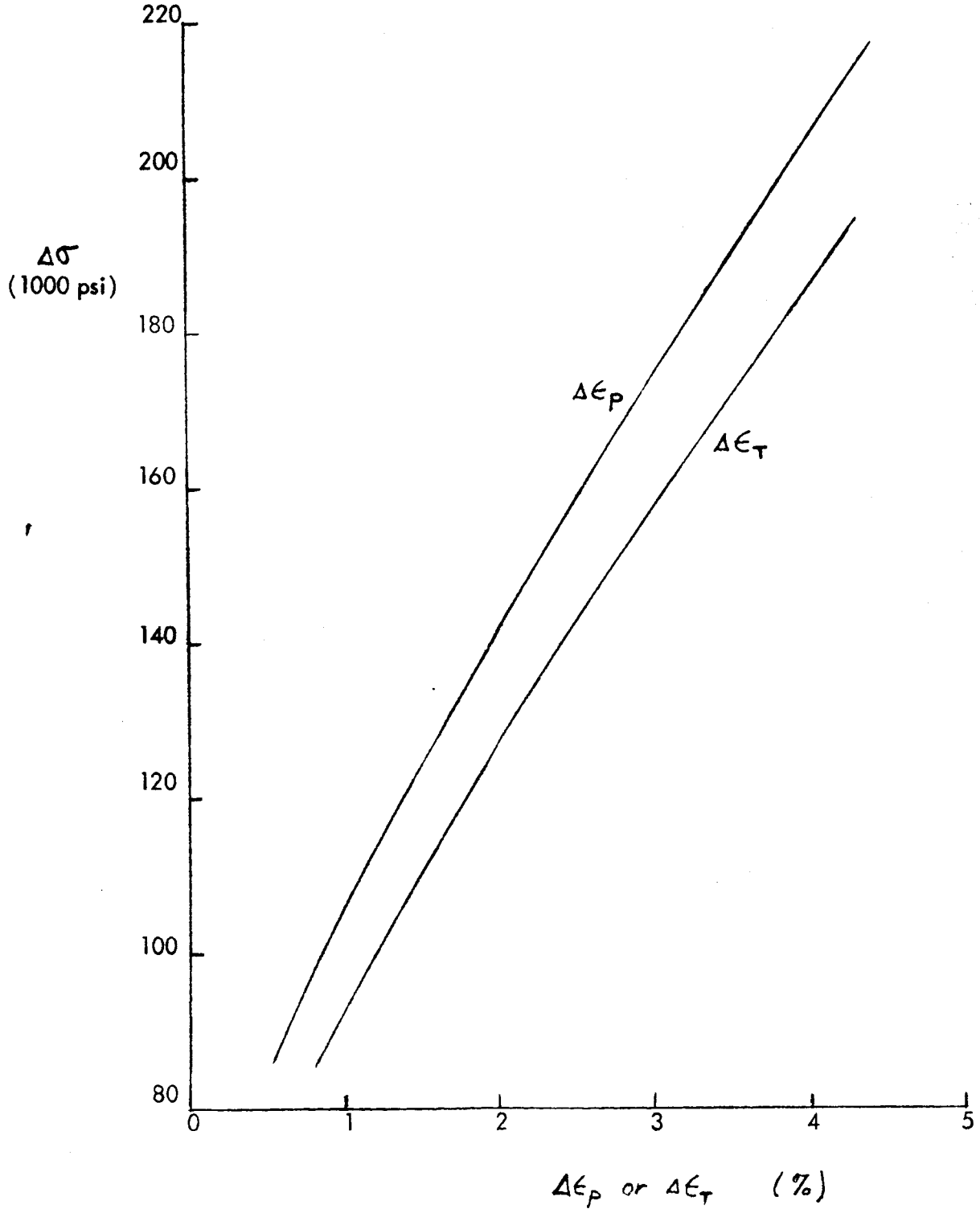

be expected to produce appreciable twist of the element as well as a reduction in fatigue life. An estimate of the relative magnitudes of the steady torsional stresses and the cyclic bending stresses can readily be obtained for an element of ideal elastic-plastic material in the form of a thin-walled tube. If τ_m is the maximum shear stress at B in Figure 1,

$$T_m = \tau_m A \frac{d}{2} \tag{12}$$

where A is the cross-sectional area of the tube. Assuming that τ_m is small relative to the axial bending stress σ, it may be further assumed that σ is the flow-stress of the material. Then,

$$\omega_p = 2\sigma \Delta\epsilon_p = 2\sigma\left(\frac{d}{R} - \frac{2\sigma}{E}\right), \tag{13}$$

and Equation (6) becomes

$$2\pi \tau_m A \frac{d}{2} = 2\sigma\left(\frac{d}{R} - \frac{2\sigma}{E}\right) A l$$

or

$$\frac{\tau_m}{\sigma} = \frac{2}{\pi}\frac{l}{d}\left(\frac{d}{R} - \frac{2\sigma}{E}\right) = \frac{2}{\pi}\frac{R}{d}\left(\frac{d}{R} - \frac{2\sigma}{E}\right)\theta_m . \tag{14}$$

Thus, for a particular total strain range d/R, the ratio of the maximum steady shear stress to the cyclic bending stress is proportional to θ_m for small values of θ_m. The distribution of shear stresses can be similarly expressed, from Equations (4) and (14),

$$\frac{\tau}{\sigma} = \frac{2}{\pi}\frac{R}{x}\left(\frac{d}{R} - \frac{2\sigma}{E}\right)\frac{\theta^2}{\theta_m} . \tag{15}$$

Equation (15) can also be written,

$$\frac{\tau}{\sigma} = \frac{2}{\pi} \frac{\Delta\epsilon_p}{\Delta\epsilon_T} \frac{\theta^2}{\theta_m} \quad . \tag{16}$$

For a particular element geometry, when θ_m is small enough so that $\Delta\epsilon_p/\Delta\epsilon_T$ is a small fraction (i.e., the hysteresis loop is narrow), Equation (16) indicates that τ_m/σ will increase rapidly with increases in θ_m, since $\Delta\epsilon_p/\Delta\epsilon_T$ also increases rapidly. Consequently, it is possible that there will exist a particular value of θ_m above which the element rapidly becomes unstable.

The foregoing results can be used to estimate the twist of the element that would be expected on the basis of classical plastic flow theory. The Prandtl-Reuss incremental flow equations (Reference 6) are expressed by

$$d\epsilon_{ij}^P = \sigma_{ij}' \, d\lambda \quad , \tag{17}$$

where $d\epsilon_{ij}^P$ and σ_{ij}' are the incremental plastic strain components and the deviator or reduced stress components, respectively, written in tensor notation, and $d\lambda$ is a scalar factor of proportionality. Consider the plastic deformation resulting during one-half revolution of the element. For the present case,

$$\left.\begin{aligned} &\sigma_{11} = \sigma \;, \quad \sigma_{12} = \sigma_{12}' = \tau \;, \quad \sigma_{22} = \sigma_{33} = \sigma_{13} = \sigma_{23} = 0 \\ &\sigma_{11}' = \sigma_{11} - \tfrac{1}{3}\left(\sigma_{11} + \sigma_{22} + \sigma_{33}\right) = \tfrac{2}{3}\sigma \\ &\Delta\epsilon_{11}^P = \Delta\epsilon_p = \frac{\alpha}{\lambda} - \frac{2\sigma}{E} \;, \quad \Delta\epsilon_{12}^P = \frac{\Delta\gamma_p}{2} \end{aligned}\right\} \;, \tag{18}$$

where $\Delta\gamma$ is the plastic shear strain increment. Equations (17) may be written in the incremental form,

$$\frac{\Delta e_{12}^{P}}{\sigma_{12}'} = \frac{\Delta \epsilon_{11}^{P}}{\sigma_{11}'} \quad . \tag{19}$$

Substitution of Equations (18) into Equation (19) yields

$$\frac{\frac{1}{2}\Delta\gamma_p}{\tau} = \frac{1}{\frac{2}{3}\sigma}\left(\frac{d}{R} - \frac{2\sigma}{E}\right) ,$$

or

$$\Delta\gamma_p = 3\frac{\tau}{\sigma}\left(\frac{d}{R} - \frac{2\sigma}{E}\right) \quad . \tag{20}$$

Substitution of Equation (15) into Equation (20) yields, for the total plastic shear strain per revolution,

$$\gamma_p = 2\Delta\gamma_p = \frac{12}{\pi}\frac{R}{d}\left(\frac{d}{R} - \frac{2\sigma}{E}\right)^2 \frac{\theta^2}{\theta_m} \quad . \tag{21}$$

The rate of twist along the element due to plastic deformation is given by

$$\frac{d\,\Delta\varphi}{ds} = \frac{2\gamma_p}{d} = \frac{24}{\pi}\frac{R}{d^3}\left(\frac{d}{R} - \frac{2\sigma}{E}\right)^2 \frac{\theta^2}{\theta_m} \quad . \tag{22}$$

Multiplying by $ds = R\,d\theta$, and integrating from θ to θ_m , the maximum twist $\Delta\varphi_m$ at θ_m is given by

$$\Delta\varphi_m = \frac{8}{\pi}\left(\frac{R}{d}\right)^2\left(\frac{d}{R} - \frac{2\sigma}{E}\right)^2 \theta_m^2 \quad . \tag{23}$$

This result may also be written,

$$\Delta\varphi_m = \frac{8}{\pi}\left(\frac{\Delta\epsilon_p}{\Delta\epsilon_T}\right)^2 \theta_m^2 \quad , \tag{24}$$

which further indicates the rapid increase expected in $\Delta\varphi_m$ with increasing θ_m for small values of θ_m and $\Delta\epsilon_p$, and the possibility of an instability "threshold."

It should be noted that in the foregoing analysis the effects of the bending moment distribution have not been included. These moments tend to cause a plastic bending deformation out of the initial plane of curvature of the element, which should also contribute to element instability.

B. Torus Device with Friction Drive

During the program it was decided to utilize the approach based on the torus device with friction drive, described previously in Reference 1. The success of laboratory tests under another NASA program to develop an attenuation strut (Reference 7) indicated that this approach could meet the requirements of the present program more simply than the torus segment approach.

The device consists, basically, of two concentric tubes separated by torus wire elements. A built-in interference between the torus wire elements and the undeformed annular space causes elastic deformation of the tube walls which produces a lateral compressive force adequate to roll the elements. The results of a theoretical and experimental program to develop design procedures and design data for stainless steel working elements is described in Reference 7 and will be briefly summarized here.

1. Analysis of Working Elements

The objective is to relate the force required to roll a torus element to the various geometric and material parameters. The energy balance of Equations (6) - (9), based on simple bending, may be written

$$\frac{f}{d} = \frac{1}{8}\,\overline{\omega_f}\,(\Delta\epsilon_r) \quad , \tag{25}$$

where f is the roll force per unit length and $\overline{\omega_p}$ is the average hysteresis. In the present device where a significant compressive force is required for adequate drive, $\overline{\omega_p}$ is a function of strain range as well as a "squeeze" factor k, defined by

$$k = \frac{f_c}{f} \quad , \tag{26}$$

where f_c is the compressive force per unit length of element. Thus, Equation (25) may be written

$$\frac{f}{d} = \frac{1}{8}\,\overline{\omega_p}\,(\Delta\epsilon_T, k) \quad . \tag{27}$$

For successful operation of the device - i.e., in order for the elements to roll rather than slide - it is required that $k > 1/\mu$, where μ is the coefficient of friction between the elements and tubes. A series of tests was performed, as described in Reference 7, to determine f/d as a function of $\Delta\epsilon_T$ and k for 300 Series stainless steel working elements. These results are shown in Figure 4. The dashed line, which corresponds to k = 0, is a semi-empirical curve based on the result of Equations (7) and (25),

$$\frac{f}{d} = \frac{\eta}{8}\,\Delta\sigma\,\Delta\epsilon_p \quad . \tag{28}$$

This equation was used with the results of Figure 3 and an average value for η determined from tests described in Section IV of this report.

2. Spacing of Elements

The compressive forces on a cluster of elements generally arise from both hoop deformation and axial bending of the tube walls. Consequently, distribution of the forces depends on the axial spacing. An analysis of

Figure 4. Design Curves for 300 Series Stainless Steel Torus Elements, Including Squeeze Effects

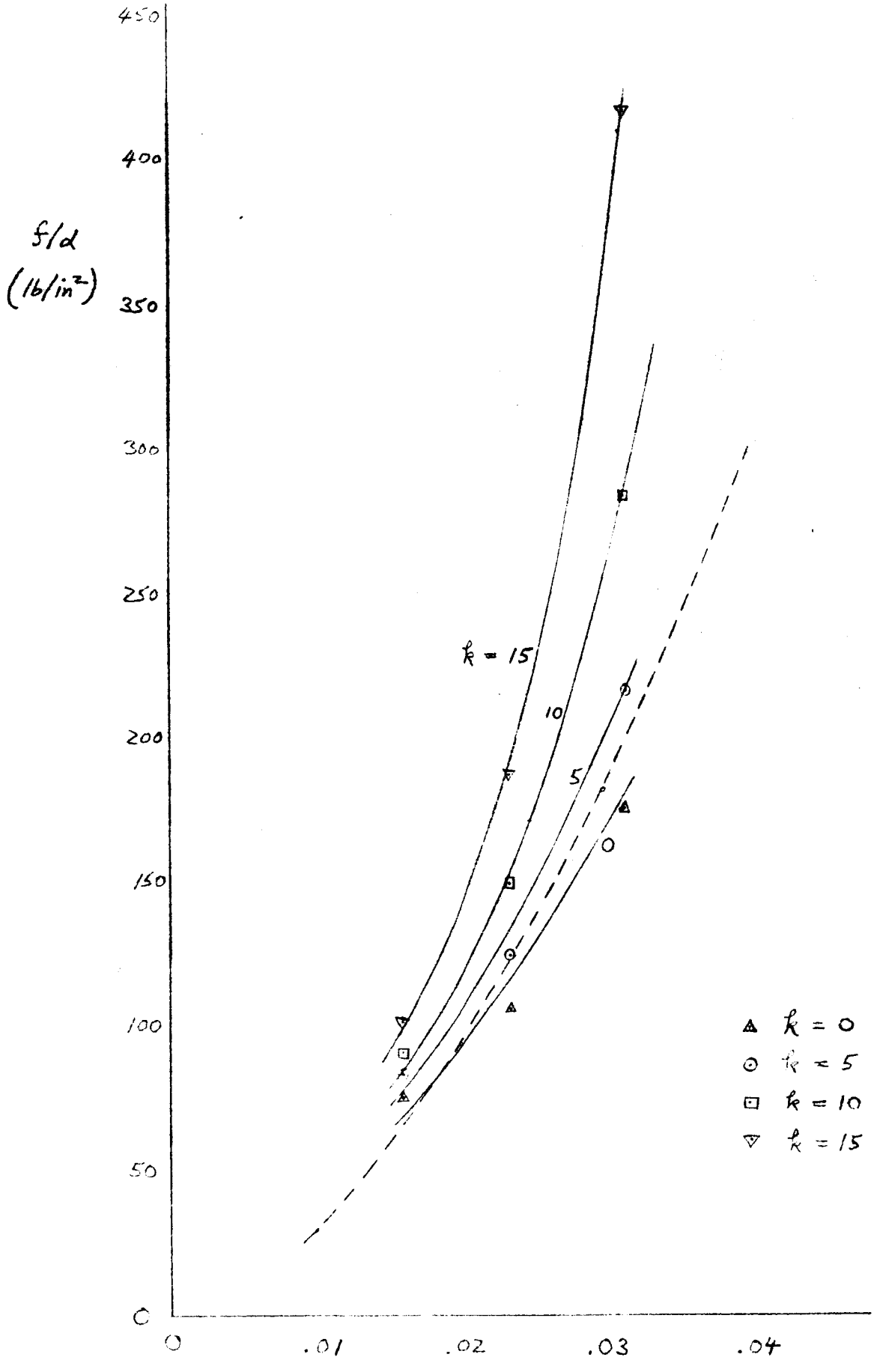

the problem is presented in Reference 7, and some of the pertinent results are described here.

Because of the effects of lateral compressive force on performance, as described in the previous section, it is desirable to maintain the force on each element at a constant design value. For an infinite cluster of elements sufficiently closely spaced, the tubes will be deformed uniformly in hoop tension and compression, and the forces on the elements will be constant and uniform. However, for finite clusters, end effects will cause a redistribution of the compressive forces. Also, spacings greater than a characteristic length will produce axial variations in the radial deflection, resulting in forces different from those based on simple hoop deformation.

The characteristic length is $1/\lambda$, where

$$\lambda = \left[3(1-\nu^2)\right]^{1/4}/\sqrt{Rt} = 1.285/\sqrt{Rt} \quad , \quad for \ \nu = 0.3 \, , \tag{29}$$

R and t are the tube radius and thickness, respectively, and ν is Poisson's ratio.

The effect of uniform spacing ℓ of an infinite cluster of elements can be described by a compression factor η_c , defined by

$$\eta_c \equiv f_c/K\ell y_o \, , \tag{30}$$

and a bending factor η_B , defined by

$$\eta_B \equiv M/M_o \, . \tag{31}$$

The factor η_c is the ratio of the actual compressive force on the element f_c to the force KLy_o produced by the radial deflection y_o in uniform hoop deformation. Here, $K = E\,t/R^2$ and E is Young's modulus for the tube material. In Equation (31), M is the bending moment in the shell at the point of contact of an element, and M_o is the reference value, $f_c/4\lambda$. M_o represents the moment produced by a single element exerting a radial force of magnitude f_c on an infinite tube. The effect of spacing is indicated in Figure 5 which shows η_c and η_B plotted against the nondimensional spacing parameter, λL . For spacings up to $\lambda L = 1$ it is seen that the deformation is very nearly uniform hoop deformation. For this case, hoop stress σ_H , compressive force, radial deflection, and element spacing can be related by

$$\sigma_H = \frac{f_c R}{Lt} = \frac{y_o E}{R} \quad . \tag{32}$$

From the foregoing results, it should be possible to approximate the force distributions of finite closely-spaced clusters by uniform pressures. In this manner the deflection distribution required to produce a uniform pressure and, hence, uniform compressive forces can be determined. It has been found that the use of a pilot element or bearing spaced some characteristic distance from the end of a finite (or semi-infinite) cluster, which produces the same radial deflection, gives rise to a nearly uniform force distribution on the cluster. This is indicated by the deflection solution shown in Figure 6 for a semi-infinite uniform pressure distribution f_c/L with a concentrated load P spaced a distance a from the end of the cluster. The concentrated load was adjusted to

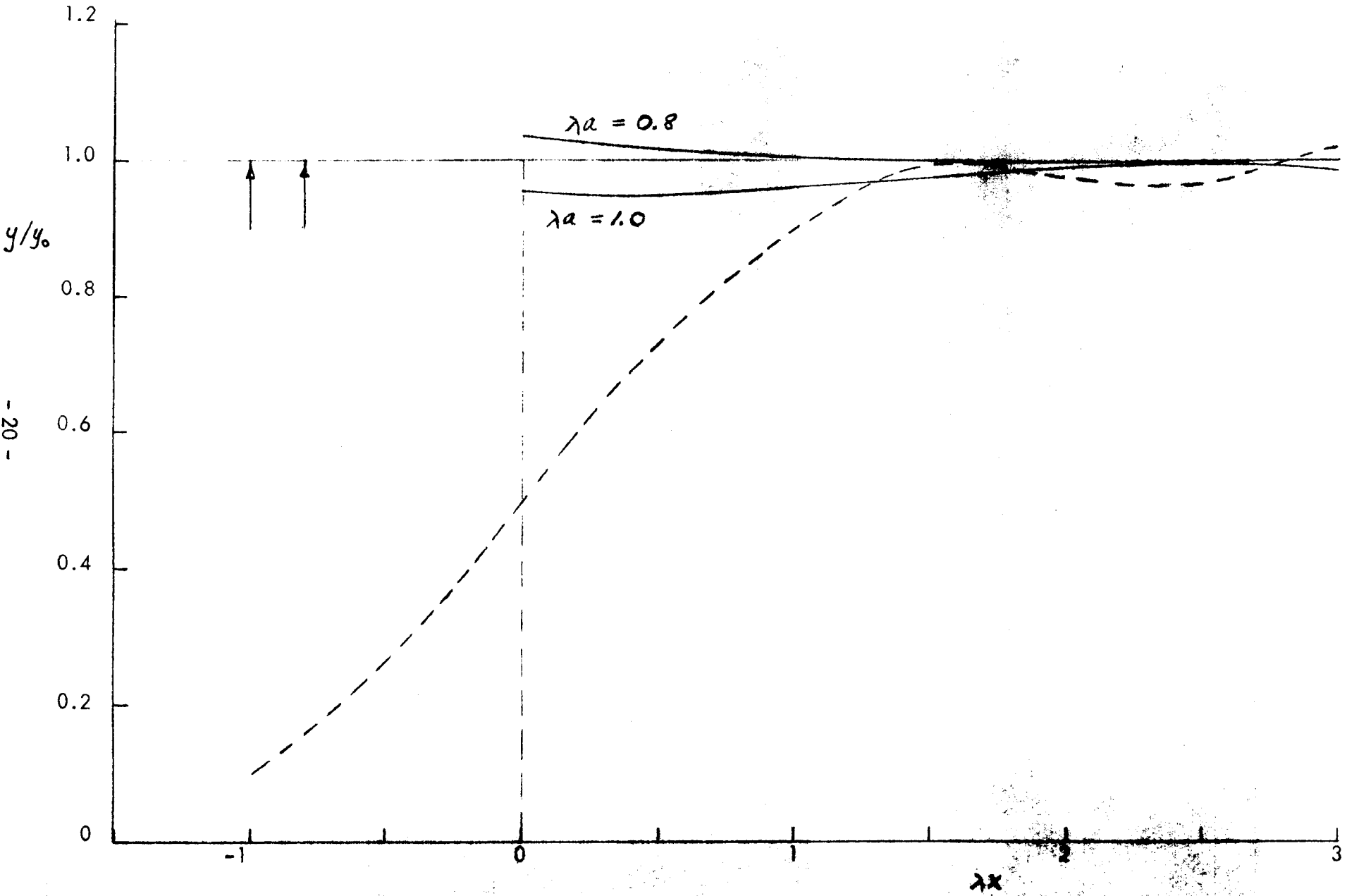

Figure 6. Deflection Distributions for Concentrated Load and Semi-Infinite Uniform Load

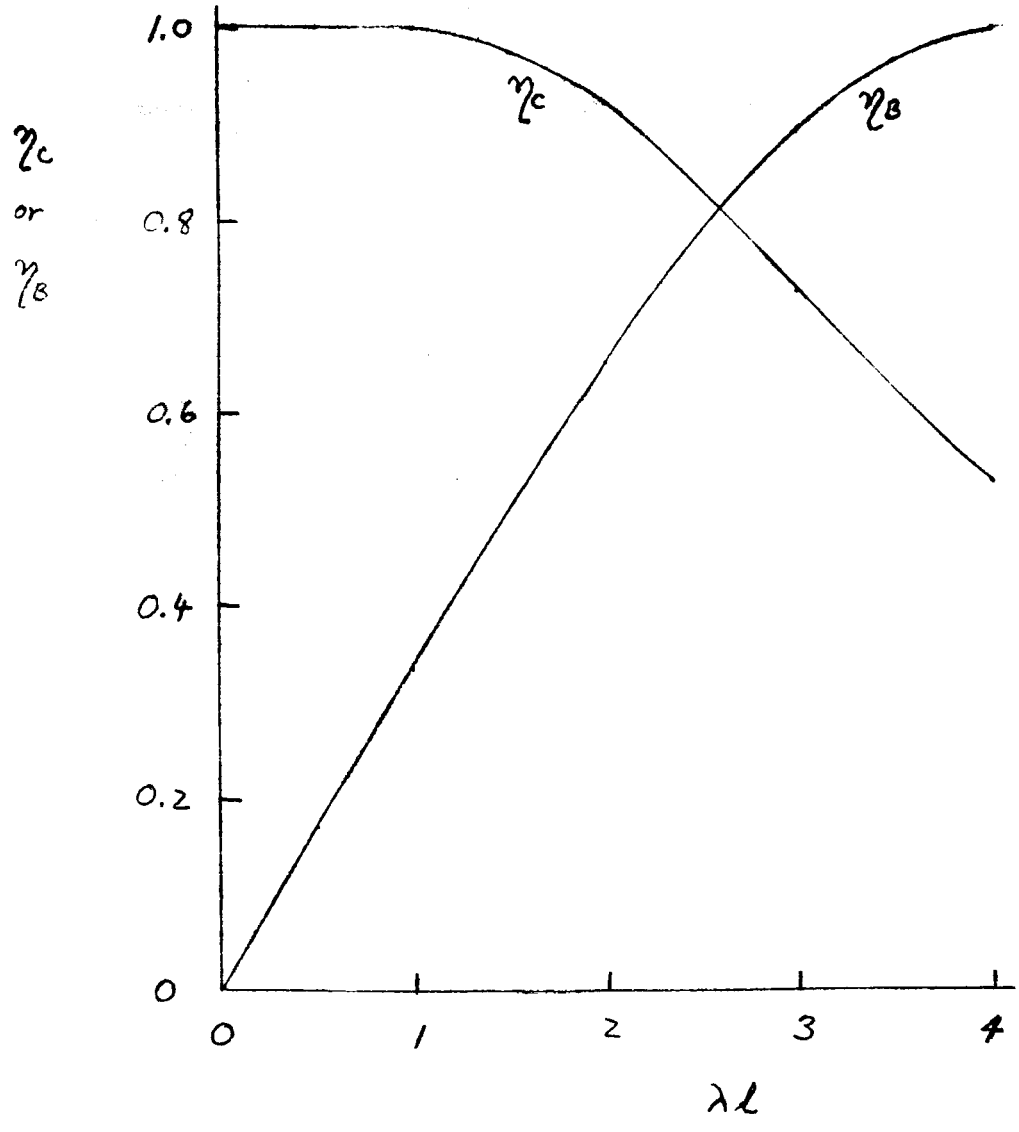

Figure 5. Compression and Bending Factors vs Element Spacing

produce the same deflection which results an infinite distance from the end of the distributed load. Two cases are shown in addition to the case of no concentrated load (dashed line). The concentrated load has a magnitude,

$$P = \frac{f_c}{\lambda \ell} (2 - D_{\lambda a}) , \tag{33}$$

and the moment M_p at the point of application is

$$M_p = \frac{f_c}{4\lambda^2 \ell} (2 - D_{\lambda a} - B_{\lambda a}) , \tag{34}$$

where

$$D_{\lambda a} = e^{-\lambda a} \cos \lambda a , \quad B_{\lambda a} = e^{-\lambda a} \sin \lambda a . \tag{35}$$

IV LABORATORY TESTS

A series of rotating beams tests was conducted to investigate the energy absorption, fatigue life, and stability of torus segment elements. Most of the tests were performed on Type 304 Stainless Steel rods, and some very limited tests were performed on copper elements.

A. Test Description

Photos of the test apparatus and test specimens are shown in Figures 7-11. The apparatus is designed to rotate rod-shaped specimens of various lengths under various curvatures or strain ranges. The specimen is mounted in two chuck-arbors and the angle of curvature is set by means of an angle-setting bar shown in Figure 7. One end of the specimen is driven at constant speed by an electric motor and the other end is connected to a counter. The rotational speed was 10 cps in all of the tests.

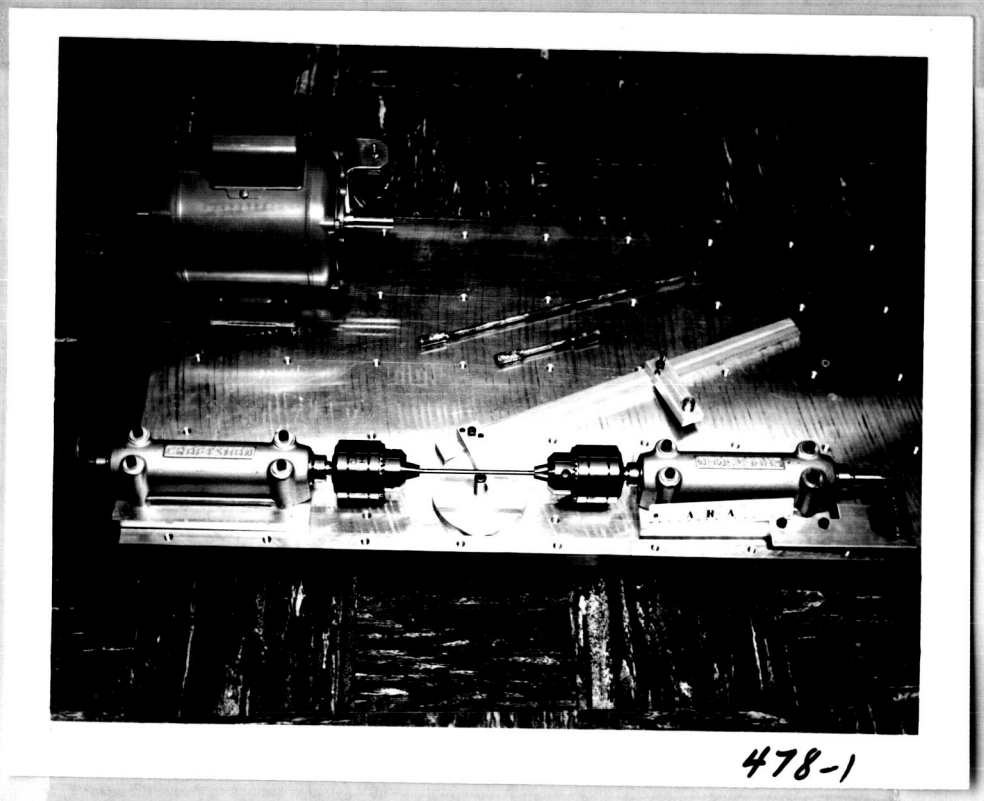

Figure 7. Test Apparatus - General Layout

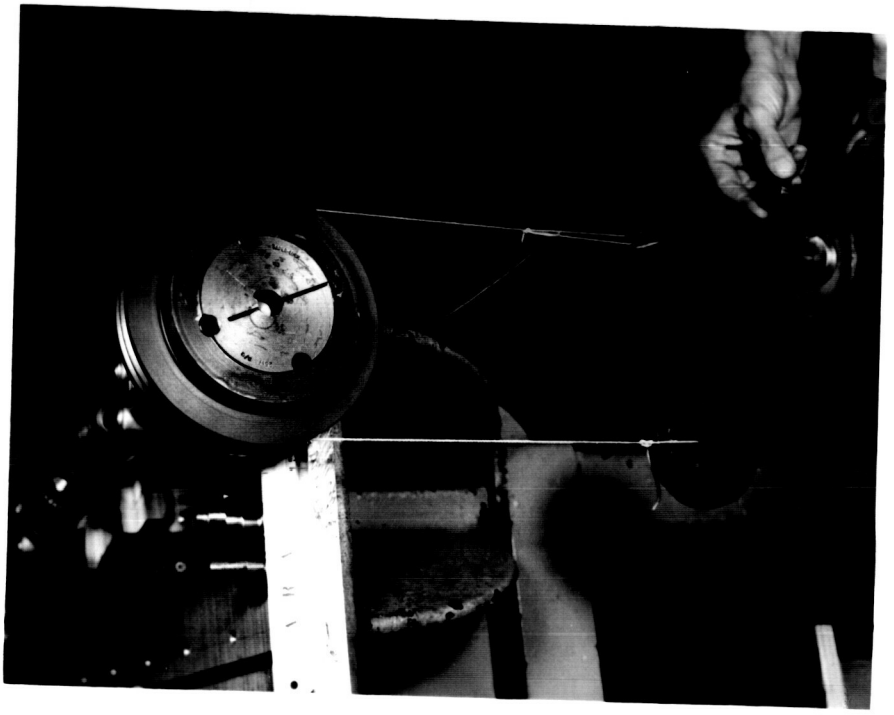

Figure 8. Torque Measurement

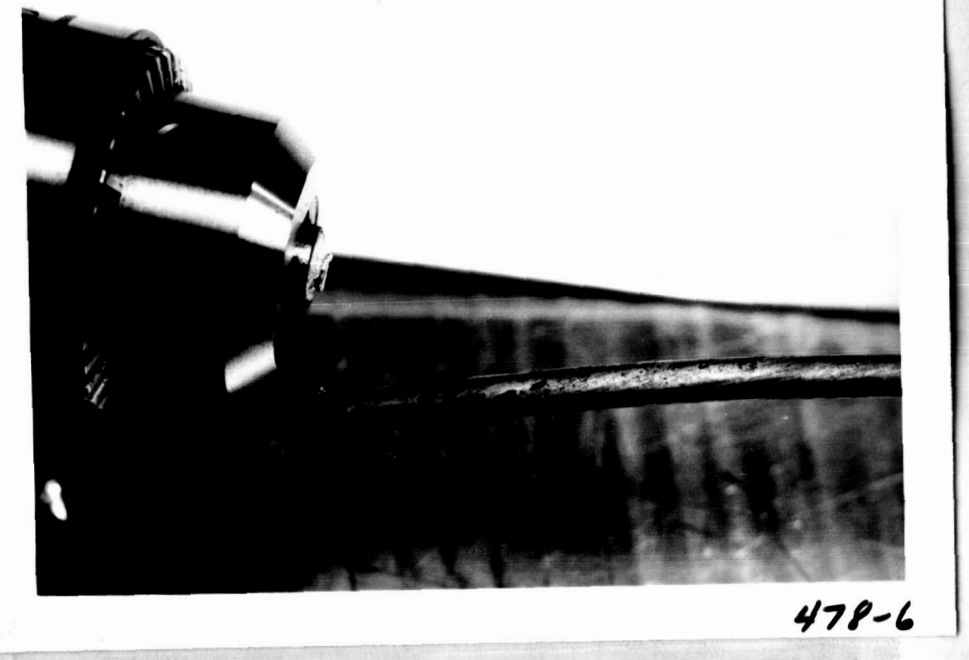

Figure 9. Failed Specimen Showing Twist

Figure 10. Failed Specimen Showing Distortion

Figure 11. Various Test Specimens

The ends of the specimens were enlarged in order to avoid stress concentrations at the grips. In most of the specimens the ends were brazed to the test rods, and a few were machined from solid stock. The test section OD was 0.25 inch in all cases.

The torque required to rotate the specimen was measured periodically during the test by dead-loading the drive pulley, as shown in Figure 8. The number of cycles in a burst was limited to control temperature rise. The temperature rise was measured periodically by means of a thermocouple thermometer held in contact with the specimen.

Each run was carried to fatigue failure, although appreciable distortion of the specimen sometimes occurred considerably before failure (Figures 10 and 11). In addition to visual observations of the distortion, the angle of twist of the specimen was measured in some cases. Figure 9 shows the twist in a specimen at failure.

B. Test Results

The pertinent test results for the stainless steel specimens are shown in Table 2. The value for T_m represents an average value during the run. In general, there was little variation in T_m except for an initial stabilizing period. The stress ranges and plastic strain ranges indicated were computed from the data of Figure 3.* In addition to the measured fatigue life N, a calculated value N_o, based on Equation (11) with $C = 0.65$ (Reference 5), is also included. Except where noted, the specimens failed at the driven end, as would be expected.

* Although the data of Figure 3 corresponds to Type 347 stainless steel, it is expected that there is little difference in stress-strain properties between this and Type 304 used for the test specimens.

TABLE 2. SUMMARY OF ROTATING BEAM TESTS WITH STAINLESS STEEL TORUS ROD SEGMENTS

Sample No.	ℓ (in.)	θ_m (deg)	T_m (lb-in.)	$\Delta\epsilon_T$ (in./in.)	$\Delta\epsilon_p$ (in./in.)	$\Delta\sigma$ (psi)	N	N_o	Specimen Type	Remarks
512	12.50	23.2	15.4875	.008098	.005167	85,000	13,900	15,825	Brazed	16° windup at 5500 cyc., 25° at 9900 cyc, slight distortion at 11,700 cyc; failed in central region.
515	6.25	11.7	7.8175	.008167	.005201	86,000	9,130	15,619	Brazed	Slight distortion and 12° windup at failure
516	12.50	46.38	55.6075	.01619	.01226	114,000	340	2,811	Brazed	Bad distortion and 285° windup at 50 cyc.; very bad distortion at failure
519	12.50	28.9	24.0425	.01009	.00690	92,500	5,320	8,874	Brazed	Bad distortion and 135° windup at failure
520	12.50	34.8	33.7775	.01215	.008684	100,500	2,310	5,602	Brazed	145° windup at 500 cyc.; very bad distortion at failure
521	2.56	9.66	11.3575	.01646	.01253	115,000	1,170	2,691	Brazed	20° windup at failure
522	2.56	7.34	6.6375	.01251	.008993	102,000	2,430	5,224	Brazed	10° windup at 2200 cyc.
523	2.56	7.34	6.6375	.01251	.008993	102,000	3,610	5,224	Machined	--
524	2.56	7.34	9.2925	.01251	.008993	102,000	1,370	5,224	Machined	Tapered diameter; failed at small end.
525	2.56	9.66	15.7825	.01646	.012494	115,000	270	2,707	Machined	Tapered diameter; failed at small end.
526	2.56	9.66	11.3575	.01646	.012494	115,000	1,850	2,707	Machined	--
527	6.25	14.68	11.6525	.01025	.007057	92,600	3,140	8,484	Brazed	Slight distortion at failure.
528	6.25	17.6	16.0775	.01229	.008821	100,600	1,500	5,430	Brazed	Slight distortion and 35° windup at failure.
529A	6.25	23.4	27.8775	.01633	.01239	114,200	970	2,752	Brazed	145° windup
530	2.56	18.0	32.8925	.03068	.02520	159,000	160	665	Brazed	15° windup at 50 cyc., 30° windup at 100 cyc., 90° windup at 150 cyc., 110° windup at failure (windup estimated).
532	2.56	18.0	32.5975	.03068	.02520	159,000	180	665	Brazed	30° windup (estimated) at 100 cyc.
533	1.00	7.85	13.7175	.03425	.02842	169,000	170	523	Brazed	45° windup (estimated) at failure.

The most significant results are shown in Figures 12 and 13. Figure 12 shows the efficiency factor η of Equation (10) plotted against total strain range. The various points are identified in terms of the specimen ℓ/d values. Figure 13 shows the ratio N/N_o plotted against strain range, for the various ℓ/d values.

It is significant that the energy absorption-characteristics of the specimens, as described by the parameter η, are relatively unaffected by strain range as well as torque and moment distributions, for the range of parameters investigated. All of the points fall within about $\pm 8\%$ of the constant value 0.38. This value was used to compute the curve in Figure 4 corresponding to $k = 0$. Of course, as the strain-range is reduced and begins to approach the elastic value, η would be expected to decrease rapidly. In fact, the values corresponding to $\ell/d = 50$ appear to indicate this trend.

The data of Figure 13 shows that an increase in strain range for a particular ℓ/d value results in a general decrease in fatigue life, based on simple bending and the relation of Equation (11). Also, the rate of decrease of N/N_o with increasing strain range appears to increase with ℓ/d value, and becomes quite rapid for the cases $\ell/d = 25$ and $\ell/d = 50$. The results are somewhat complicated by the appreciable distortion of the specimens which sometimes occurred prior to failure, and the attendant variations in strain distributions. The rapid decrease in N/N_o with strain range is consistent with the results of Moyar and Sinclair and the idealized plastic stability analysis of Section III, in which plastic

Figure 12. Efficiency Parameter, η, for 300 Series Stainless Steel Torus Rod Segments

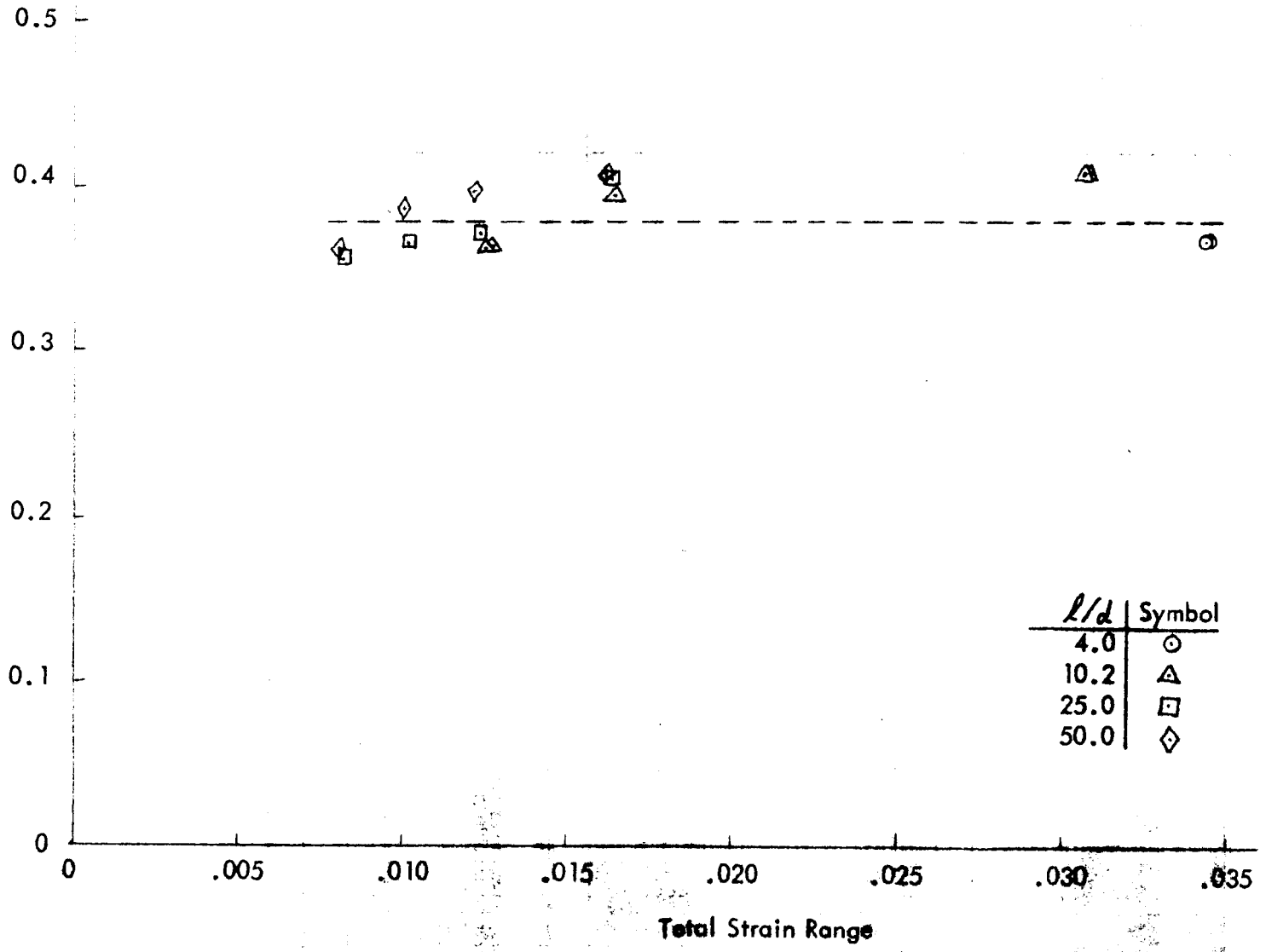

Figure 13. Fatigue Life for 300 Series Stainless Steel Torus Rod Segments

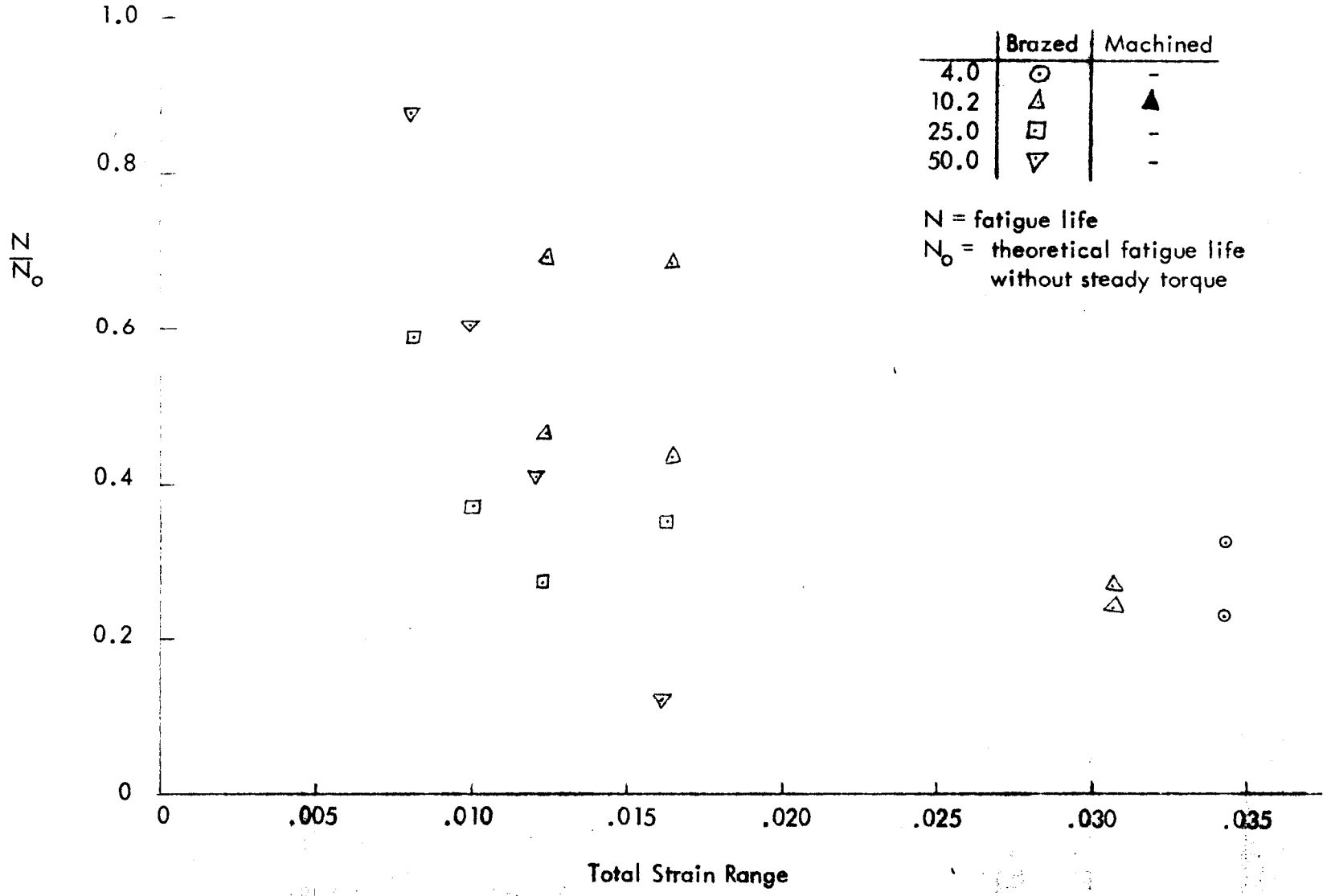

torsional windup of a tube was predicted as a function of θ_m. For a particular ℓ/d value, total strain range is proportional to θ_m.

The results for the two machined specimens suggest the possibility that the corresponding brazed specimens were introducing strain concentrations. However, the data is too limited to be conclusive, particularly in view of the scatter normally associated with fatigue data.

Because of the change in design approach from a torus segment to a friction-drive torus device, as previously discussed, the scope of the program did not permit completion of the rotating beam tests as originally planned. Consequently, tests with stainless steel and copper tubes, which were to provide a quantitative evaluation of the previous stability analysis, could not be conducted. Moreover, the data obtained from the tests with copper specimens is too limited to be of significance.

V DESIGN AND FABRICATION

Five energy absorber units utilizing the friction-torus principle were designed and fabricated to meet the requirements of Table 3. The Type C unit design

Table 3. Design Requirements

Unit Type	Quantity	Load Level (lb)	Stroke (in.)
A	1	3,300	10
B	1	53,300	10
C	3	53,300	36

included provisions for load adjustment through replacement of a cartridge containing the loaded torus elements. These units are to be shipped to Marshall Space Flight Center where they will undergo a series of static and dynamic tests. Descriptions of the units and summaries of the pertinent design parameters are presented below.

A. Type A Energy Absorber

This unit is a simple constant-force energy absorber consisting of inner and outer tubes, torus cluster, and end fittings. Photos of the device are shown in Figures 14 to 16, and a summary of pertinent design parameters is presented in Table 4. The torus cluster shown in Figure 15 consists of split wire elements separated by flat wire spacers. The pilot elements at each end consist of caged rollers which take the increased bearing load and insure uniform alignment of the cluster.

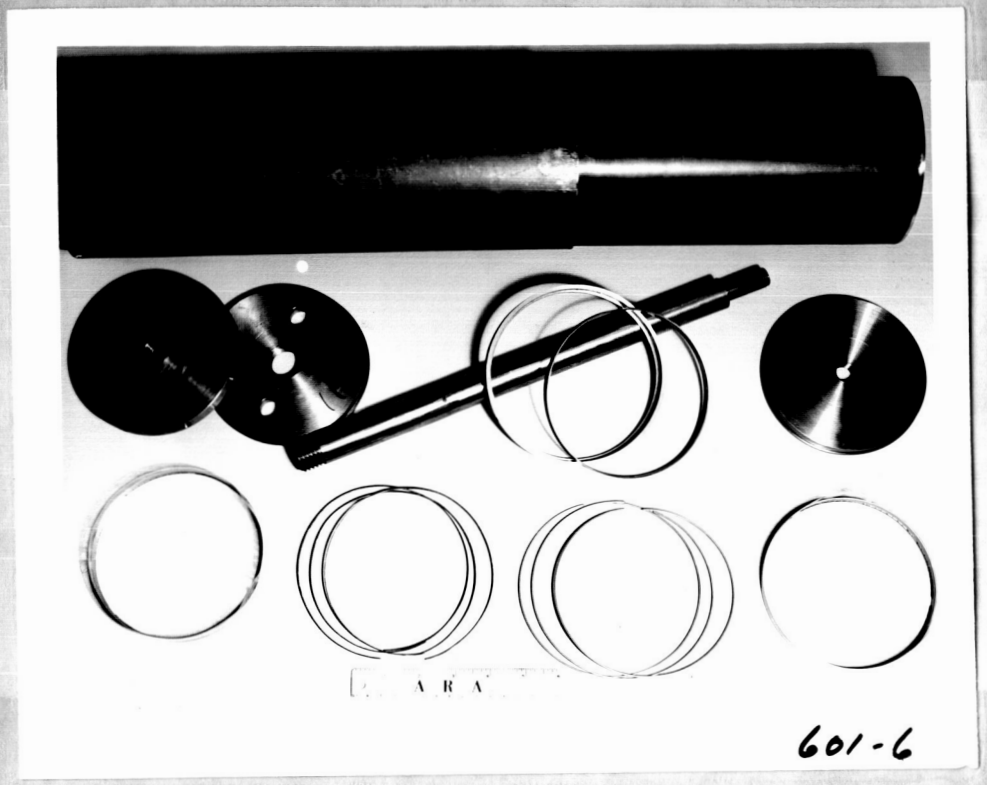

Figure 14. Type A Energy Absorber Components

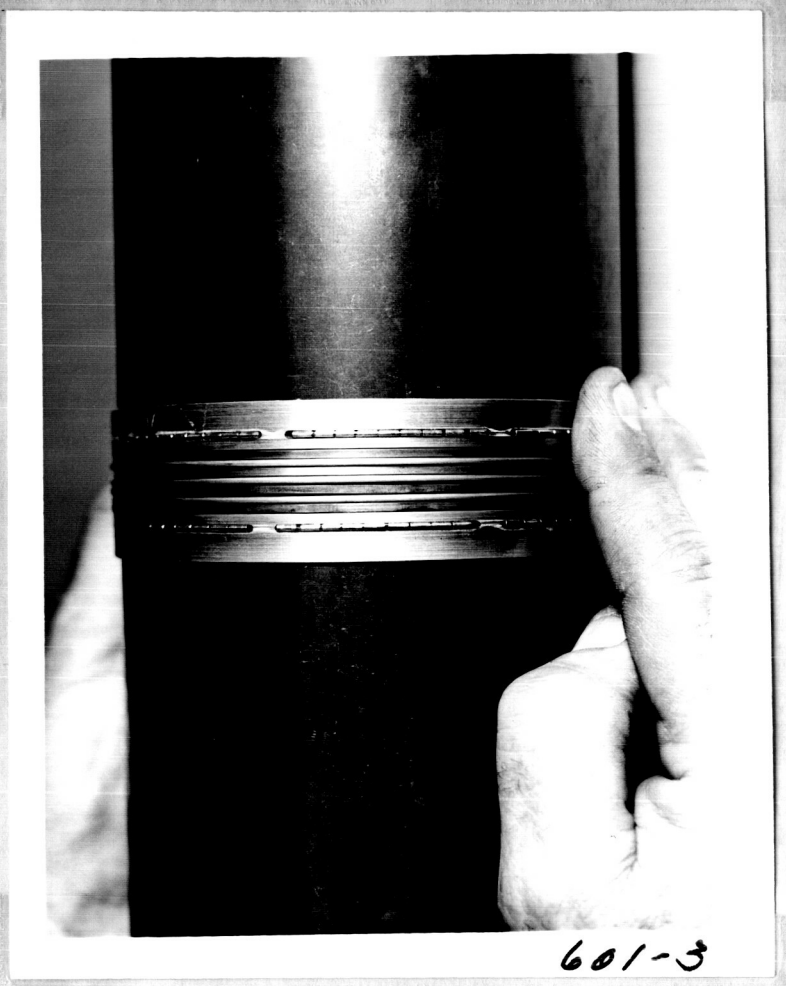

Figure 15. Type A Energy Absorber -- Torus Cluster

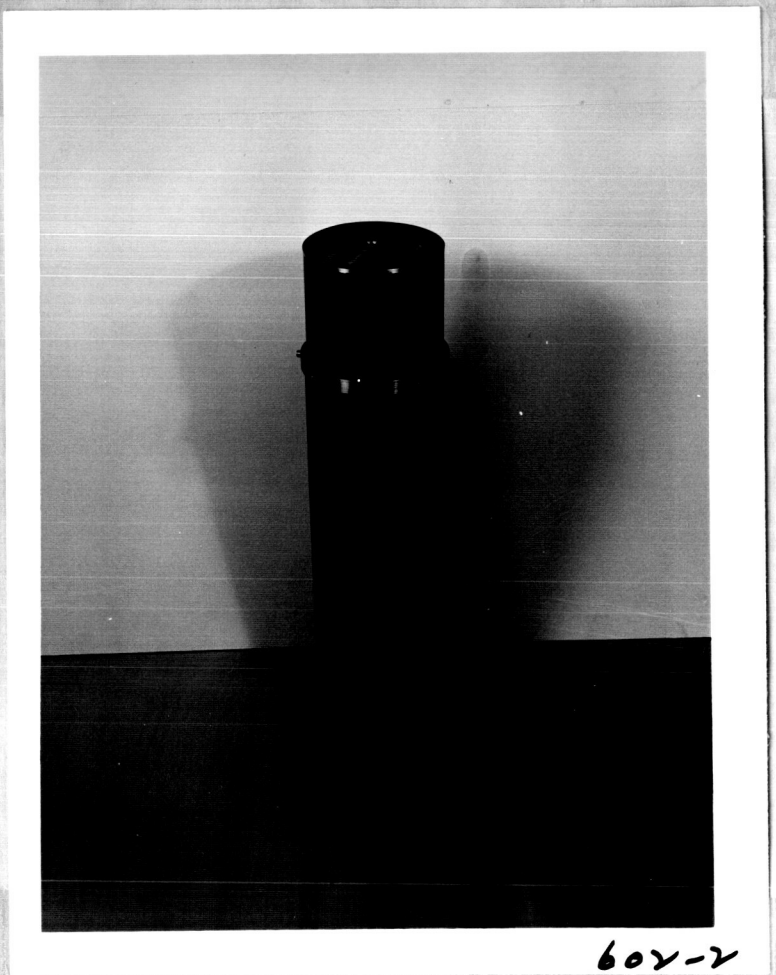

Figure 16. Type A Energy Absorber -- Completed Assembly

Table 4. Type A Energy Absorber Design Summary

Tubes

Material:	17-7 PH Stainless Steel
Thickness:	0.032 in.
Radius:	2.5 in. (nominal)
Radial deflection:	0.005 in.
Hoop stress:	59,000 psi
Bending stress:	76,000 psi

Torus Clusters

Torus element material:	Type 304 Stainless Steel
Element diameter:	0.063 in.
Strain range:	2.5%
Roll force per element:	170 lb
Squeeze factor:	10
Spacer width:	0.083 in.
Pilot spacing:	0.178 in.
Roller diameter:	0.063 in.
Roller length:	0.180 in.

B. Type B and Type C Energy Absorbers

Type C unit is a constant-force energy absorber with means provided for replacing a cartridge containing the torus elements, and thereby changing the load level. Type B unit is a constant force energy absorber similar in construction to Type C unit, except for its non-segmented tubes and shorter length.

A detail design drawing of Type C unit is shown in Figure 17. The inner and outer tubes are axially segmented in three sections and keyed together to form continuous surfaces for the rolling torus elements. The middle segment contains the torus elements and the outer segments provide for the necessary stroke length. The tube segments are held together by inner and outer rings of tie rods connected to the end fittings. This design permits the unit to be readily disassembled so that the middle cartridge can be replaced for load adjustment.

The inner middle tube is split, axially, to facilitate loading of the torus elements. The torus cluster, similar in design to that of Type A unit, is assembled in place, and the inner tube is expanded radially and locked in place by inserting a key in the axial slot.

A summary of pertinent design parameters for the Type C energy absorber is presented in Table 5.

Table 5. Types B and C Energy Absorber Design Summary

Inner Tubes	
Material	Mild steel clad with Type 304 stainless steel
Thickness:	0.300 in.
Radius:	6 in. (nominal)
Radial Deflection:	0.003 in.
Outer Tubes	
Material:	17-7 PH stainless steel
Thickness:	0.100 in.
Radius:	6 in. (nominal)
Radial deflection:	0.009 in.
Hoop stress:	45,000 psi
Bending stress:	59,000 psi
Torus Clusters	
Torus element material:	Type 304 stainless steel
Element diameter:	0.135 in.
Strain range:	2.25%
Roll force per element:	713 lb
Squeeze factor:	10
Spacer width:	0.115 in.
Pilot spacing:	0.542 in.
Roller diameter:	0.135 in.
Roller length:	0.380 in.

VI CONCLUSIONS AND RECOMMENDATIONS

The development program described herein has served to produce advanced energy absorbing devices utilizing the cyclic material deformation concept. It has also served to extend the state-of-the-art in energy absorbing devices through the development of units capable of multiple operation in tension and compression, adjustment for load level, and other attractive features.

Some limited investigation of performance has already been conducted, and a test program is planned by the Marshall Space Flight Center. However, a broad evaluation program would be desirable to establish the true capabilities of these devices over a range of design and performance conditions. Three important areas of investigation for successful application to the space program are as follows:

1. Fatigue and Endurance Behavior

Fatigue and endurance limits of torus devices should be established as a function of the pertinent design and performance parameters such as strain range, lateral compressive forces, materials of construction, cyclic rate, and temperature rise. It is also important to determine variations in force level and load-stroke behavior as a function of the above mentioned parameters, particularly under repeated operation.

2. Effects of Space Environment

It is important to determine the effects of a space environment on performance. In particular, effects of severe vacuum-thermal exposure on the rolling of torus elements under friction drive should be established. The use of dry film lubricants and metallic coatings might also be included in such an investigation.

3. Effects of Non-Axial Loading and Vibration Environments

In most space applications of load-attenuation struts, the devices will be subjected to bending moments, torques, etc., in addition to axial tension and compression loads. In some cases severe vibration environments can also be expected. It is important to determine the effects of these added loads on performance, and to establish the limits of load-carrying capability as a function of the various design parameters.

REFERENCES

1. Platus, D.L., et al, "Concepts of Multiple-Impact Study of Energy Absorption," Final Report, Contract No. NAS 7-226, ARA Report #49. 31 October 1964.

2. Moyar, G. J. and G. M. Sinclair, "Cyclic Strain Accumulation under Complex Multiaxial Loading," RTD-TDR-63-4120, Dec. 1963.

3. Coffin, L. F., Jr., "The Stability of Metals Under Cyclic Plastic Strain," General Electric Research Laboratory, Report No. 56-RL-2137, November 1958.

4. Tavernelli, J. F. and L. F. Coffin, Jr., "A Compilation and Interpretation of Cyclic Strain Fatigue Tests on Metals," Transactions, American Society for Metals, Vol. 51, 1959, pp. 438-453.

5. Coffin, L. F., Jr. and Tavernelli, J. F., "The Cyclic Straining and Fatigue of Metals, "Met. Soc. AIME, Trans., Vol. 215, October 1959, pp. 794-806.

6. R. Hill, The Mathematical Theory of Plasticity. London: Oxford University Press, 1950.

7. Platus, D. L., et al, "Development and Qualification of an Attenuation Strut," Four Month Interim Report, Contract No. NAS 9-3533, ARA Report #57, 15 February 1965.

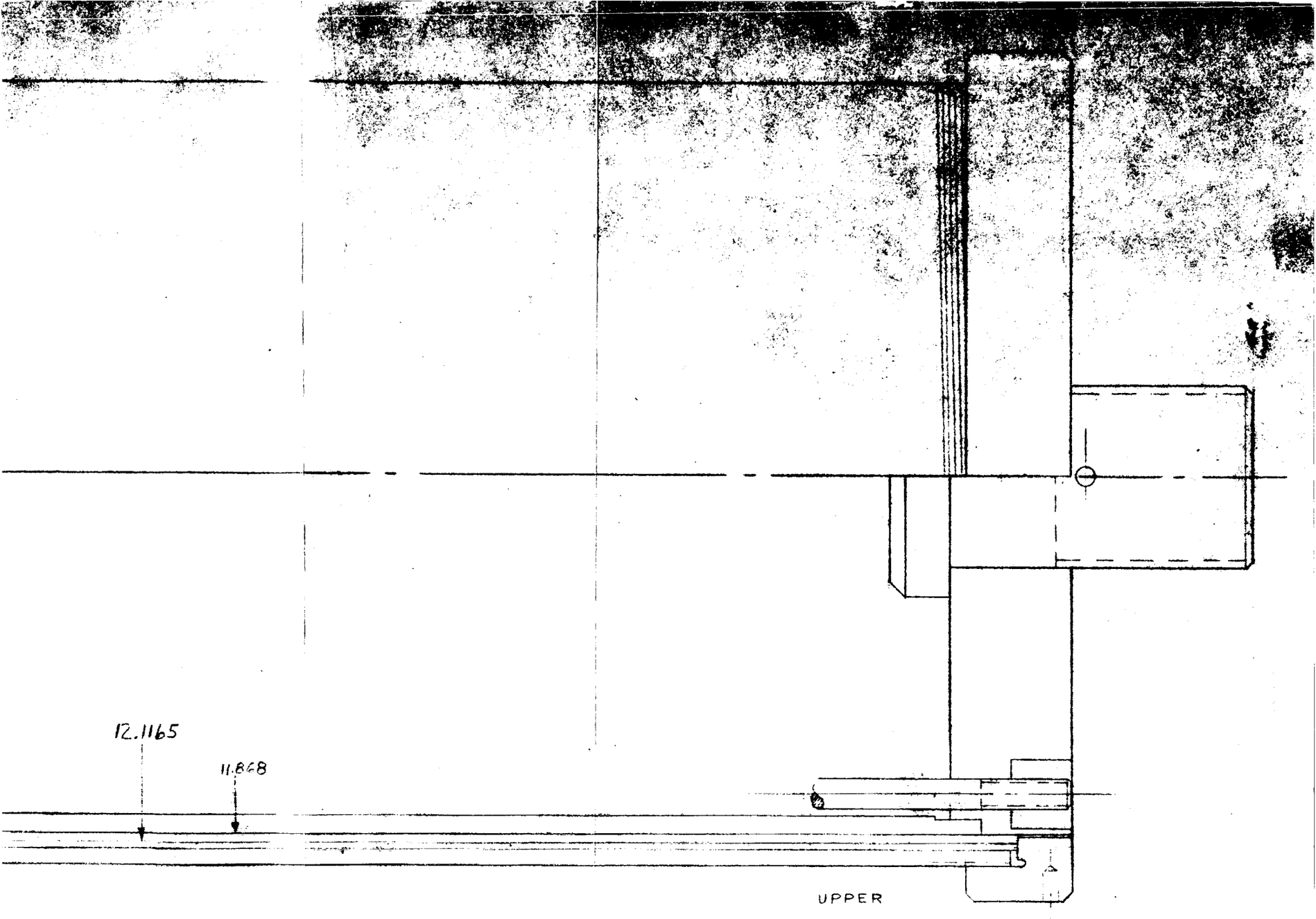

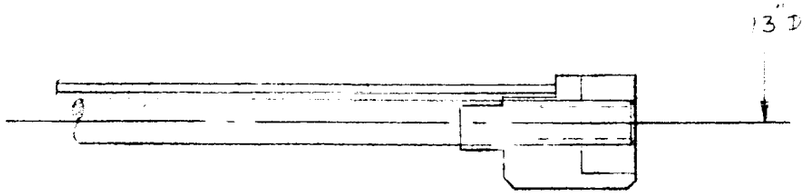

A R A, inc.

West Covina California

DEVICE
12-36-53 M

DO NOT SCALE DRAWING

Scale	1:2	Date
Drwn	HF 3-5-65	
Engr		
Appd	RJC 3-6-65	
File No.	24	issued

D-1200

12.000

LOWER